J Mol Model (2011) 17:607–619
DOI 10.1007/s00894-010-0755-z

ORIGINAL PAPER

Modeling and analysis of the compatibility of polystyrene/poly(methyl methacrylate) blends with four inducing effects

Dan Mu · Jian-Quan Li · Yi-Han Zhou

Received: 8 February 2010 / Accepted: 1 April 2010 / Published online: 5 June 2010
© Springer-Verlag 2010

Abstract The compatibility of polystyrene (PS) and poly (methyl methacrylate) (PMMA) blends was studied over a wide range of compositions at 383, 413 and 443 K, respectively, by atomistic and mesoscopic modeling. All the calculated Flory–Huggins interaction parameters showed positive values; furthermore, they were all above the critical Flory–Huggins interaction parameter value, which means that the PS/PMMA blends were immiscible. Both the addition of a block copolymer and the introduction of a shear field influenced the phase morphologies of the blends, while the degree of influence depended on the compositions of the blends. The study of PS/PMMA blends doped with nanoparticles showed that the mesoscopic phase was influenced by not only the properties of the nanoparticles, such as their size, number and number density, but also the compositions of the blends. The effect of the surface roughness of the planes on the phase separation of the blends was also studied.

Keywords PS/PMMA blend · Inducing effect · Phase morphology · Nanoparticle

D. Mu (✉)
Department of Chemistry, Zaozhuang University,
Shandong 277160, China
e-mail: mudanjlu1980@yahoo.com.cn

J.-Q. Li
Physics and Electronic Engineering Department,
Zaozhuang University,
Shandong 277160, China

Y.-H. Zhou
National Analytical Research Center of Electrochemistry
and Spectroscopy, Changchun Institute of Applied Chemistry,
Chinese Academy of Sciences,
Changchun, China

Introduction

Polymer blend systems play an important role in the plastic industry because they can be tuned to have a better combination of physical properties than the corresponding homopolymers. The process of physical blending is much easier to perform than chemical blending (e.g., grafting), and the former is also more economical. As a general rule, the aim of blending is to obtain a product with new or better properties. Because of the different physical properties of candidate polymers, it is not always easy to obtain completely miscible polymer mixtures. When the components of polymers can form energetically favorable interactions, such as hydrogen bonding, dipole interactions, etc., it is possible to obtain a miscible blend. For immiscible blends, adding interferents is a common method of changing the microscopic morphology. This improves the blend miscibility and thus enhances its properties.

Polystyrene (PS) and poly(methyl methacrylate) (PMMA) are conventional model systems in polymer science. PS/PMMA blends are a well-known immiscible combination [1-8], and their bulk and surface phase separation has been observed [9, 10]. Immiscible blends are known to have properties combining those of their component polymers, and also to have segregated structures with domains that are predominantly formed from the individual homopolymers. It has been shown that changing the relative homopolymer proportions in such blends can change the domain structure, surface morphology, and even the phase morphology [11-13].

Some contradictory results can be found in the literature regarding the miscibilities of certain polymers and the possibility of predicting miscibility from surface tension or from parameters derived from it. These contradictions can be attributed to several reasons. Firstly, the structures and

the properties of partially miscible polymer blends depend on the processing conditions used, which may influence conclusions about polymer compatibility when they are deduced from macroscopic properties or from the structure of the blend. Secondly, methods that can be used to predict miscibility are limited [14, 15]. For example, various experimental difficulties can be encountered during the determination of the Flory–Huggins interaction parameter, χ, which can be used to characterize the strength of the interaction between the polymers. χ can be determined by various methods, such as inverse gas chromatography, solvent diffusion, or the dependence of composition on mechanical properties, but all of these methods have their drawbacks. Finally, when blend systems have two calorimetric T_g values, it does not necessarily indicate that their components are immiscible [16]. Fortunately, computer calculations and simulations have become available as efficient methods of solving these experimental problems.

This paper is divided into two main parts. The first part is about the calculation of typical thermodynamic parameters, such as the solubility parameter, of the studied systems via a microscopic calculation method, and comparing those calculated parameters with experimental data in order to maintain a high level of accuracy in further calculations and simulations; the second part describes mesoscopic dynamics simulations of several kinds of inducing effects that can change the phase morphologies of PS/PMMA blends. Mesoscale structures are of the utmost importance during the production processes of many materials, such as polymer blends, block copolymer systems, surfactant aggregates in detergent materials, latex particles, and drug delivery systems.

Mesoscopic dynamics models have been receiving increasing attention recently, as they form a bridge between microscale and macroscale properties [17-20]. Mesoscopic dynamics (MesoDyn) [21-23] and dissipative particle dynamics (DPD) [24, 25] methods both treat the polymer chain at a mesoscopic level by grouping atoms together and then coarse-graining them to be persistent-length polymer chains. These two mesoscopic modeling methods increase the scale of the simulation by several orders of magnitude compared with atomistic simulation methods. MesoDyn utilizes dynamic mean-field density functional theory (DFT), in which the dynamics of phase separation can be described by Langevin-type equations to investigate polymer diffusion. Thermodynamic forces are found via mean-field DFT, using the Gaussian chain as a model. The most important molecular parameter is the "incompatibility parameter" χN, where χ is the Flory–Huggins interaction parameter and N is the degree of polymerization.

However, owing to the soft interaction potential of the DPD method, it is not suitable to apply the DPD method in our work, especially when dealing with the interactions between blending materials and planes or doped nanoparticles. Furthermore, in the study of the compatibility of PEO/PMMA blends in our former work, the MesoDyn simulation method was successfully applied to detect the phase morphologies of PEO/PMMA blends. From a theoretical point of view, these results clarified several conflicting conclusions of different experiments [26]. Therefore, the MesoDyn method has been shown to be reliable when dealing with PS/PMMA blends. The mesoscale simulation process used in this paper was carried out with the MesoDyn module in the Material Studio commercial software provided by Accelrys.

Simulation details, results and discussions

This paper consists of two parts: calculations performed via (1) molecular dynamic (MD) simulations and (2) mesoscopic simulations. The intermediate parameter connecting the microscale and the mesoscale is the Flory–Huggins parameter, χ. MD simulation is used to accurately study bulk polymer properties when this is difficult to do experimentally. Although MD simulation is widely used nowadays, it is difficult to detect the phase separation of blends via a microscopic method, such as MD simulation. Therefore, it is necessary to combine it with a mesoscopic method, such as MesoDyn simulation, to perform a full study of polymer blends from the microscale to the mesoscale.

Atomistic molecular simulation

Model and simulation

The selection of the representative chain length (N_{mon}) was our primary task. This simulation process was carried out at room temperature (298 K) on an SGI workstation by following the MD procedure in the commercial Cerius2 package program provided by Accelrys.

The simulation processes (including the construction of the models) were the same for both PS and PMMA, so we will use an atomistic chain length N of 10 for PS as an example here to describe the simulation process in detail. Initially, the proposed polymer chain structure was generated using the rotational isomeric state (RIS) model of Flory [27], which describes the conformations of the unperturbed chains. Three PS polymer chains were then generated following the same principle, each with ten repeating units; they were then put into a simulation box with a density of 1.05, which is the density of bulk PS [28]. Minimization was then done using the conjugate gradient method (CGM) with a convergence level of 0.1 kcal mol^{-1} $Å^{-1}$ until the energy reached a minimum. This minimized configuration was refined by MD simulation for 30 ns under constant temperature and density (NVT ensemble). A time step of 1 fs was used to ensure the

stability of simulation. The Nosé–Hoover [30] thermostat in a canonical ensemble was used to create the canonical molecular dynamics trajectories, and the COMPASS force field was chosen to deal with such a condensed state system [31-33]. The spline treatment of van der Waals (VDW) interactions was chosen, with a spline window of between 11 and 12 Å. The Ewald summation [34], an accurate method of calculating long-range interactions, was applied in order to calculate long-range electrostatic interactions. Next, the refined polymer was annealed in the temperature range from 383 K (above 373 K [28], the T_g of PS) to 443 K (below 513 K [28], the melting temperature T_m of PS) in steps of 10 K for 50 cycles. The simulation time for each annealing cycle was set to 2 ns, and the system was minimized at the beginning of each annealing cycle. Because such oligomers always have strong end–end interactions, a system consisting of oligomers is different from a real polymeric system. Thus, an MD simulation was executed with the NPT (with constant temperature and pressure) ensemble for 20 ns; furthermore, MD simulations with a repeating ensemble cycle from NVT to NPT were carried out three times with a simulation time of 20 ns for each cycle to reduce the end–end interactions sufficiently. Finally, an MD simulation was executed with the NVT ensemble for 30 ns at 298 K to collect data. In general, about 200 ns was needed in total for each simulated case. During the whole simulation process, the selection of the appropriate force field was a crucial task for obtaining accurate information about the structures and dynamics of the blends. The COMPASS force field has been shown to be a suitable choice for calculating solubility parameters, especially for polymeric systems [35].

Results and discussion

The cohesive energy density (CED) of each pure component was used to calculate the solubility parameter, δ, according to the equation below:

$$\delta = \sqrt{CED} = \sqrt{\frac{E_{coh}}{V}},$$

To determine the minimum representative polymer chain length of the blend components, N_{mon}, cases with different chain lengths, N=10, 20, 30, 40, 50, 60, 70 and 80 for both PS and PMMA, were selected in order to calculate the δ value of each component. Figure 1 displays the dependence of δ of PS on the number of repeating units of PS. It can be seen that a nearly constant value is approached when the number of repeating units reaches 30, and the values are 8.32% smaller than the experimental data. This may result from the presence of a bulky C_6H_5 group in PS, which restricts free rotation around the C–C bond of its backbone. Figure 2 shows the calculated δ values for different

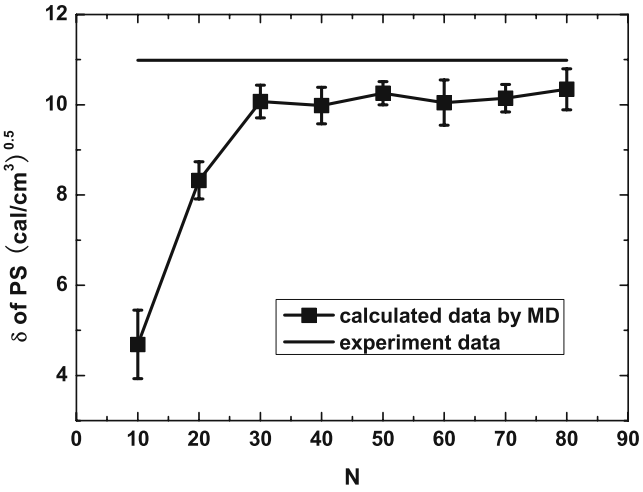

Fig. 1 The solubility parameter for different PS chain lengths

numbers of repeating units of PMMA. These become constant from N=60 onwards, and they are 6.40% smaller than the experimental results. This may result from the presence of a bulky CH_3 group in PMMA, which also restricts free rotation around the C–C bond of its backbone.

The fact that the calculated relaxation times were shorter than the experimental results presented a rather difficult obstacle to overcome in the simulations. However, taking N=60 to represent the whole polymer chain for PMMA appeared a reasonable approach. Hence, the minimum representative polymer chain lengths of PS and PMMA, N_{mon}(PS) and N_{mon}(PMMA), were chosen to be 30 and 60, respectively. Figure 3 shows a flowchart that illustrates the process described above.

The blend systems were binary, with PS (density = 1.05 gcm^{-3}) and PMMA (density = 1.188 g cm^{-3}) as the components. The glass transition temperature of PS is

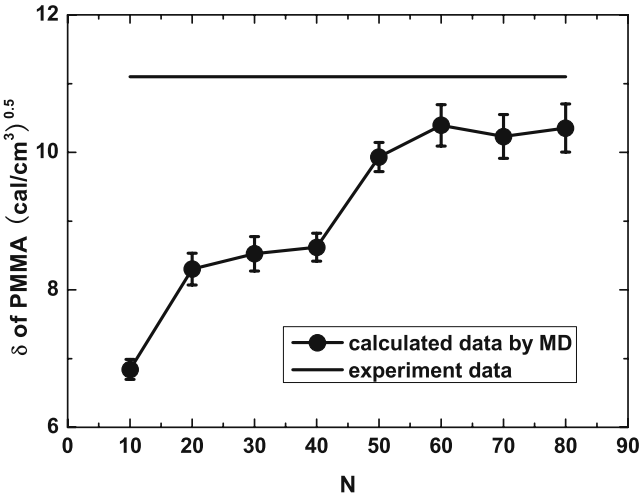

Fig. 2 The solubility parameter for different PMMA chain lengths

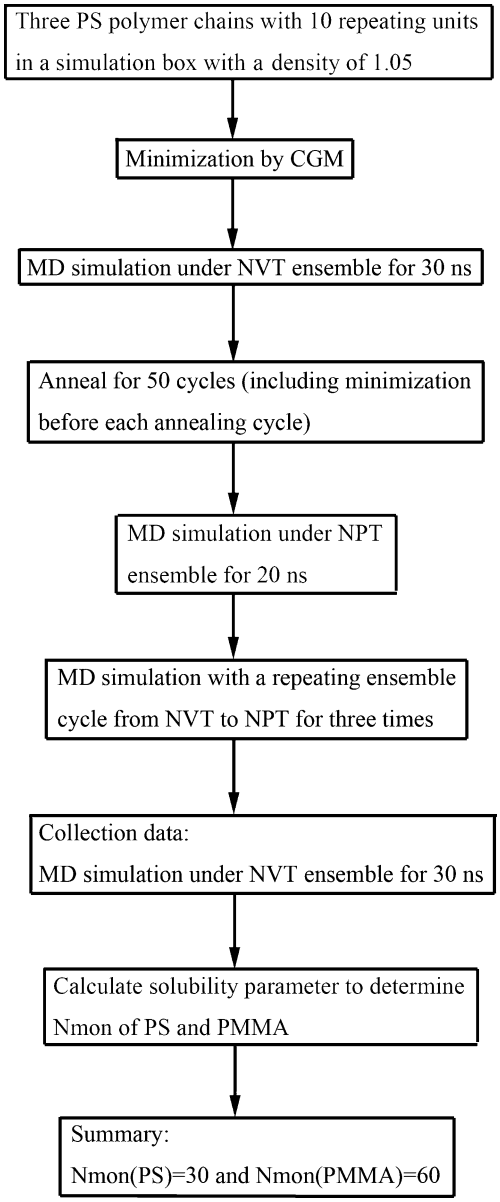

Fig. 3 The procedure used to select N_{mon} for PS

373 K, so PS is prone to crystallize at a low temperature. PMMA starts to soften at the glass transition temperature (T_g=378 K), and does not substantially depolymerize until 453 K [36]. Therefore, the blending simulation temperatures adopted were 383, 413 and 443 K.

PS/PMMA blends with different weight percentages of PS were put in a three-dimensional (3D) periodic boundary simulation box with the corresponding density. Table 1 describes the blending models in detail, including the molar ratios of PS to PMMA, the chain number per unit cell, the compositions by weight, and the densities. The blend properties calculated in subsequent studies depend on how well the components are blended. Therefore, when the blending model was generated, if the PS and the PMMA chains were randomly distributed in the simulation box, the model was assumed to be a well-mixed model and accepted for further simulations; otherwise, it was discarded, and a new blending model was built until the component chains contacted each other sufficiently. Figure 4 shows a typical 1/1 blend. Because of the end–end interactions of short polymer chains, the initial amorphous structure of the blend must first be minimized. The subsequent simulation process was the same as that used to calculate δ values for the pure components, and the simulation temperatures were also 383, 413 and 443 K.

The tendency for binary polymer chains to mix depends on the cohesive energies of the blends and their pure components. Both are applied to calculate the χ parameters of blends with different compositions. The χ parameter is defined as

$$\chi = \left(\frac{\Delta E_{mix}}{RT}\right) V_{mon},$$

where V_{mon} is the unit volume of one monomer. Here, V_{mon} equals 165.54 cm^3 mol^{-1} for blends of PS/PMMA. ΔE_{mix} for a binary mixture is defined as

$$\Delta E_{mix} = \phi 1\left(\frac{E_{coh}}{V}\right)_{pure1} + \phi 2\left(\frac{E_{coh}}{V}\right)_{pure2} - \left(\frac{E_{coh}}{V}\right)_{mix},$$

where ϕ is the volume fraction, and the subscripts "pure" and "mix" denote the cohesive energy densities of the pure components and the binary mixture, respectively. χ is shown as a function of the PS volume fraction in Fig. 5. Several features of these data are impressive. Firstly, the three χ curves vary in almost the same way at different temperatures, which means that temperature was not an efficient factor for changing the degree of phase separation. This is a totally different conclusion from that obtained for PEO/PMMA blends, which are miscible [26]. Secondly, the χ value shows a decreasing trend as the volume fraction of PS increases, except for the 1/4 blend case, where it shows a small rising trend. Then the 4/1, 6/1 and 8/1 blend cases also show another decreasing trend in χ. These two decreasing trends are termed T1 and T2, respectively. Considering the absolute data on slope variation for T1 and T2, where T1 < T2, it is supposed that the degree of phase separation would intensify with increasing PS content when the blends have a higher content of PS. In addition, the 1/4 and 4/1 blend cases produced outstandingly high χ values for both the T1 and the T2 lines, which means that it is possible that extremely distinct phase separation was present in these two blend cases.

A positive χ value alone cannot prove that the blends are immiscible; it is necessary to calculate the critical value of χ via the equation below:

$$(\chi_{AB})_{critical} = \frac{1}{2}\left(\frac{1}{\sqrt{m_A}} + \frac{1}{\sqrt{m_B}}\right)^2,$$

Table 1 Details of the PS/PMMA blend cases carried out via MD simulation

Number	System	Content	wt% of PMMA	p(gcm^{-3})
1	Pure PMMA	1PMMA chain	100	1.1880
2	1/6	1PS, 6PMMA	92.02	1.1772
3	1/4	1PS, 4PMMA	88.49	1.1724
4	1/3	1PS, 3PMMA	85.22	1.1681
5	1/2	1PS, 2PMMA	79.36	1.1604
6	1/1	1PS, 1PMMA	65.78	1.1429
7	2/1	2PS, 1PMMA	49.01	1.1220
8	3/1	3PS, 1PMMA	39.06	1.1099
9	4/1	4PS, 1PMMA	32.46	1.1021
10	6/1	6PS, 1PMMA	24.27	1.0925
11	8/1	8PS, 1PMMA	19.38	1.0868
12	Pure PS	1PS chain	0	1.0500

where m_A and m_B represent the actual number of repeating units of PS and PMMA, respectively. When the calculated and the critical values of χ are based on the same reference volume, $\chi_{AB})_{critical}$ can be used to estimate the compatibility of the blends. The blends are miscible if $(\chi_{AB})_{calculated} < (\chi_{AB})_{critical}$. In this case, the Gibbs free energy, ΔG_m, is negative. In contrast, when $(\chi_{AB})_{calculated} \gg (\chi_{AB})_{critical}$, the blends are totally immiscible; the phases will even separate. When the difference between $\chi_{AB})_{calculated}$ and $\chi_{AB})_{critical}$ is small or even zero, the blends will be partially or even totally miscible. The value of $\chi_{AB})_{critical}$ in our studied PS/PMMA blends was 0.0486, which was much smaller than the calculated χ values. Therefore, we can see that the PS/PMMA blends were immiscible at 383, 413 and 443 K.

As long as the calculated χ_{AB} and the corresponding critical values are based on the same reference volume, comparing the calculated χ_{AB} with critical values will provide useful information about the degree of miscibility of the blends. Therefore, χ_{AB}, rather than the enthalpy of mixing ΔH_m, could be used to characterize the miscibility of polymer blends [37].

However, it is also necessary to calculate thermodynamic parameters such as entropy, enthalpy and Gibbs free energy (G) to illustrate the phenomenon of polymer blending. The entropy change upon mixing long polymers is so small that the mixing enthalpy becomes a key influence on the degree of mixing. The entropy change upon mixing, ΔS_m, must be considered in addition to the enthalpy of mixing. Hence, it was important to compute ΔH_m in order to study the miscibilities of the PS/PMMA blends using the following equation [37]:

$$\Delta \mathrm{H_m} = \mathrm{V_m}\left[\left\{(\mathrm{CED})_{\mathrm{PS}}^{0.5} - (\mathrm{CED})_{\mathrm{PMMA}}^{0.5}\right\}\right]^2 \phi\mathrm{PS}\phi\mathrm{PMMA},$$

where V_m is the total volume of the blend. The CED values used to compute ΔH_m were obtained from the data in the MD simulations.

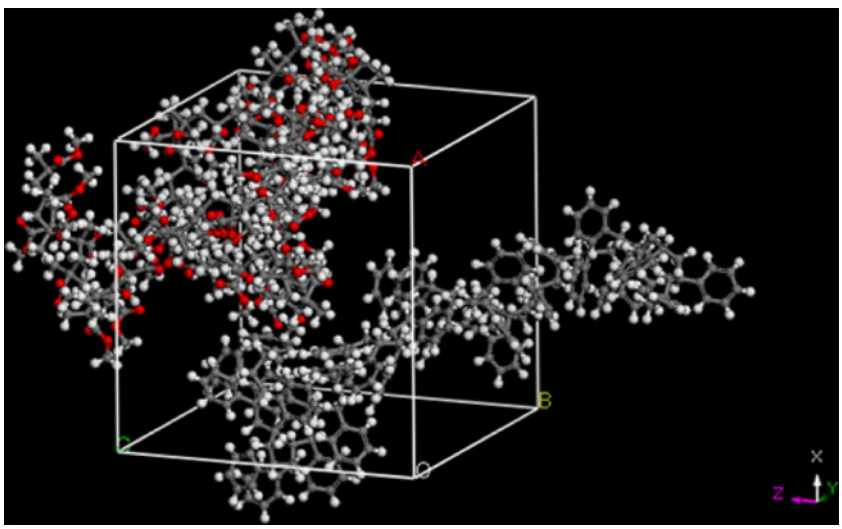

Fig. 4 Amorphous cell from the 1/1 PS/PMMA blend case. *Red*, O; *gray*, C; *white*, H

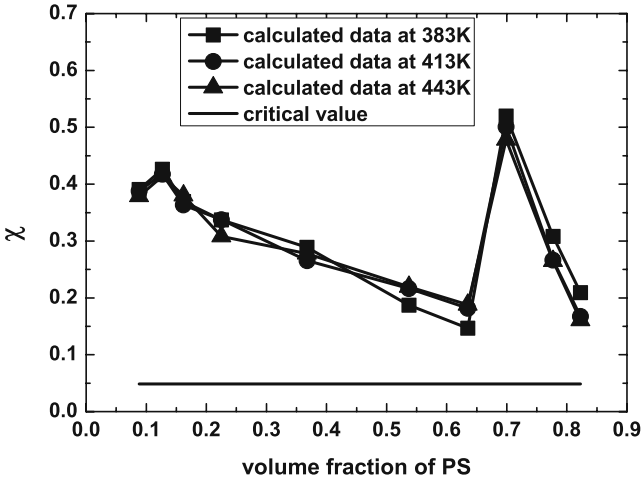

Fig. 5 Flory–Huggins interaction parameter χ as a function of the PS volume fraction for binary blends of PS/PMMA at 383, 413 and 443 K, respectively

To calculate ΔG_m, the change in entropy during mixing, ΔS_m^{comb} was needed, and this was calculated using the combinatorial entropy term for binary systems via Flory–Huggins theory [38] for two-component systems, as given by

$$\Delta S_m^{comb} = -R[\chi_A \ln \chi_A + \chi_B \ln \chi_B].$$

Thus, by using the thermodynamic formula

$$\Delta G_m = \Delta H_m - T\Delta S_m^{comb},$$

it was possible to calculate the Gibbs free energy of mixing. Both ΔG_m and ΔH_m exhibited similar trends at 413 K over the entire composition range, as shown in Fig. 6. The extreme values of these two curves both appeared in the 1/1 blend case. It is presumed that when the molar proportions of PS and PMMA are the same, such as in the 1/1 blend,

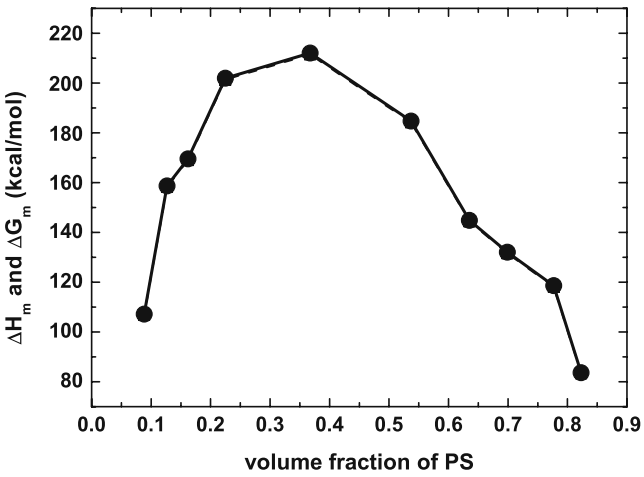

Fig. 6 Changes in enthalpy ΔH_{mix} *(solid curve)* and Gibbs free energy ΔG_{mix} (*dotted curve*) with volume fraction of PS

they exhibit the strongest attractive or repulsive interactions. Because of the low entropy of mixing, polymeric blends are mostly incompatible, and their phases will separate under the appropriate conditions. Therefore, it is necessary to carry out further research from a dynamic point of view at the mesoscopic level to study how the phase separations of PS/PMMA blends are influenced by certain inducing effects.

Mesoscopic simulation

PS/PMMA blends with a block copolymer and a shear field

To map the representative polymer chains onto Gaussian chains, the bead number (N_{meso}) and the unit chain length of the Gaussian chain (a_{meso}) are estimated by

$$N_{meso} = \frac{N\text{mon}}{C\infty},$$
$$a_{meso} = a_{mon}C\infty,$$

where N_{mon} is the number of repeating units in the polymer chain. a_{mon} is the reference unit monomer length, and $C\infty$ is the characteristic ratio of a chain of infinite length. N_{mon} was determined by the representative chain lengths of PS and PMMA, i.e., N_{mon}=30 for PS (M_W=3200) and N_{mon}=60 for PMMA (M_W=6000), while $C\infty$(PS)=9.85 and $C\infty$(PMMA)=8.65 were found in the *Polymer Handbook* [29]. The connection between the microscale and the mesoscale is as follows:

$$\nu^{-1}\varepsilon_{ij} = \chi_{AB}RT,$$

where the parameter χ_{AB} is calculated by atomistic simulation for each blend composition at different temperatures. R is the molar gas constant, 8.314 J mol^{-1} K^{-1}, and T is the simulation temperature. The calculated χ values for various compositions were all positive at 383, 413 and 443 K. N_{meso} and $\nu^{-1}\varepsilon_{ij}$ are the input parameters used in MesoDyn simulations to describe the number of Gaussian beads and the interaction between beads. In the 1/1 blend case, the N_{meso} values for PS and PMMA were 3 and 6, respectively.

In order to stabilize the numerical calculation, the time step for MesoDyn calculation, τ, was chosen to be 100 ns, and the total simulation time was 1000 μs for each blend case. A default noise parameter value of 75.002 was used for numerical speed and stability. The grid dimensions adopted were 32×32×32 nm. Ten mesoscopic simulations were carried out with different PS/PMMA blend compositions, 1/1, 1/2, 1/3, 1/4, 1/6, 2/1, 3/1, 4/1, 6/1 and 8/1 in molar ratio, which roughly covered the whole composition range.

Results and discussion

The order parameter, denoted *P*, is defined as the average difference between the local density squared and the overall density squared, as given by the equation

$$P_i = \frac{1}{V}\int_V \left[\eta_i^2(r) - \eta_i^2\right] dr,$$

where η_i is the dimensionless density (volume fraction) of species *i*. The larger the value of the order parameter, the stronger the phase separation. A decrease in *P* indicates better compatibility or miscibility, and the polymer phases mix more randomly.

It should be pointed out that the *P* data calculated by mesoscopic simulation can only be compared for the same blend composition. Therefore, plain PS/PMMA blends were used as reference cases, and their order parameter data were labeled "*A*;" in addition, the order parameter data of PS/PMMA blends of the same compositions as for the "A" blends but with inducing effects, such as being doped with a block copolymer or nanoparticles, or having planes introduced, were labeled "*B*." The value of $(B - A)/A$ is termed the variation rate of order parameters (*V ROP* for short). By comparing the *V ROP* values, we can detect which factor is the most effective at changing the phase morphology.

In order to study the influence of the addition of a block copolymer on the phase morphology, a block copolymer made of PS and PMMA with a volume fraction of 10% was added to each blend. Generally speaking, when block copolymers of the same composition are added to an immiscible blend, the compatibility of the blend will be enhanced. However, in our study, two opposite results were obtained when the block copolymer was added: an enhancement of or a deterioration in compatibility were both observed.

Several striking features of these data can be seen in Fig. 7. First, the *V ROP* values of blends with less PS (the 1/1, 1/2, 1/3, 1/4, 1/6, 2/1 and 3/1 blend cases) fluctuated around zero, and this trend was most obvious for the 1/1, 1/3 and 1/6 blend cases, which means that adding a block copolymer to the blends with less PS did not result in an obvious inducing effect. However, obvious enhancing effects were seen for the blends with more PS (the 4/1, 6/1 and 8/1 blend cases). This result can be attributed to the difference in the self-diffusion coefficients between PS and PMMA and the difference in their self-compatibility properties. Second, the *V ROP* values of the 1/2, 1/1 and 2/1 blend cases were negative at 383 K; when the temperature was increased to 413 K, the *V ROP* value of the 1/3 blend case turned from positive to negative. When the temperature was raised again, to 443 K, the *V ROP* value of the 3/1 blend case also turned from positive to negative. Based on this information, and using the 1/1 blend case as a reference, the *V ROP* values of pairs of blend cases (such as the 1/3 and 3/1 blend cases) turned from positive to negative as the temperature was gradually increased. Following this principle, when the temperature was raised above 443 K, the *V ROP* values of the 1/4 and 4/1 blend cases would be expected to become negative. The three pictures inserted into Fig. 7 are the phase morphologies of the 6/1 blend case with block copolymers added at 443, 413 and 383 K (top to bottom, respectively).

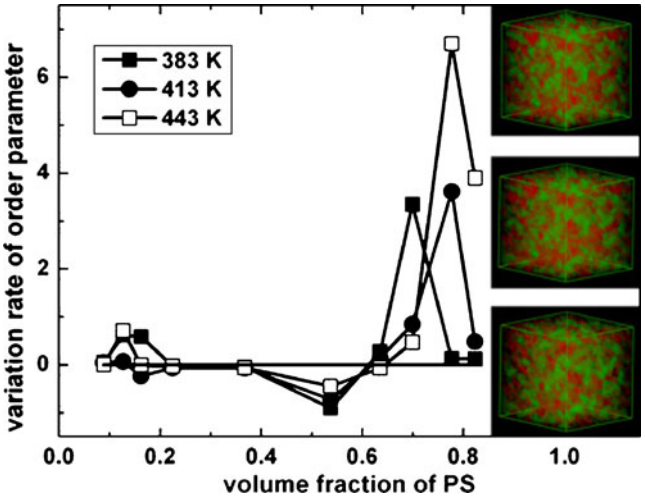

Fig. 7 *V ROP* value versus volume fraction of PS for ten blend cases with 26 block copolymers added. The zero point on the Y axis was set as the reference line. When the data are above this line, it means that the block copolymer has an enhancing effect on the PS/PMMA blend; when the data are below this line, it has a deteriorating effect on the blend. Isodensity surface pictures of a 6/1 (PS/PMMA) blend at 443, 413 and 383 K are displayed from *top to bottom* in the chart, respectively. *Red*, PS; *green*, PMMA

In order to investigate the influence of the shear field on the microscopic phase morphology, the shear rate was set to 0.001 ns^{-1} and 0.002 ns^{-1} as examples of low and high shear effects. Simulations were then performed on the basis of plain PS/PMMA blends with P data used as a reference. It can be seen from Fig. 8 that low shear stress can have a significant inducing effect on PS-rich blends, such as in the 4/1 and 6/1 blend cases. Phase separation can clearly be seen in the inserted pictures. However, shear stress had no obvious effect on the 8/1 blend case. When the shear rate was increased to 0.002 ns^{-1}, all of the *V ROP* values for the ten different blend cases were high, as shown in Fig. 9, which means that high shear stress plays an important role in changing the microscopic phase morphology, especially in PS-rich blends. In addition, the *V ROP* value of the 8/1 blend case was relatively high. Furthermore, the phase morphologies of all the blends exhibited obvious phase separation. In a word, the higher the shear rate, the more obvious the phase separation.

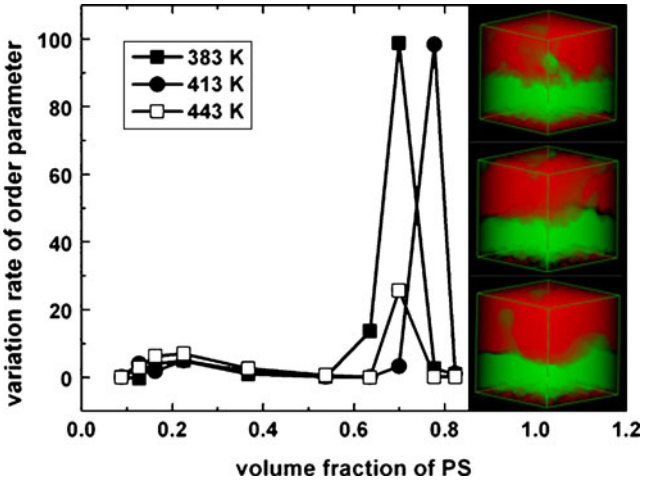

Fig. 8 *V ROP* data based on plain blends versus the volume fraction of PS. Isodensity surface pictures of a 4/1 (PS/PMMA) blend induced by a shear rate of 0.001 ns^{-1} are also shown, as are isodensity surface pictures of a 4/1 (PS/PMMA) blend at 383, 443 and 413 K (*top to bottom* in the chart, respectively). *Red*, PS; *green*, PMMA

PS/PMMA blends doped with nanoparticles

The pairs of blend cases, such as the 1/3, 3/1 and the 1/2, 2/1 blend pairs, were then used as examples to study the inducing effect of doping with nanoparticles. In addition, the 1/3 (with a PS volume fraction of 16.21%) and 1/2 (with a PS volume fraction of 22.49%) blend cases were used to represent compositions rich in PMMA, while the 2/1 (with a PS volume fraction of 53.72%) blend case was used to represent compositions that contain roughly equal amounts of PS and PMMA, and the 3/1 (PS volume fraction of 63.52%) blend case was chosen to represent compositions rich in PS.

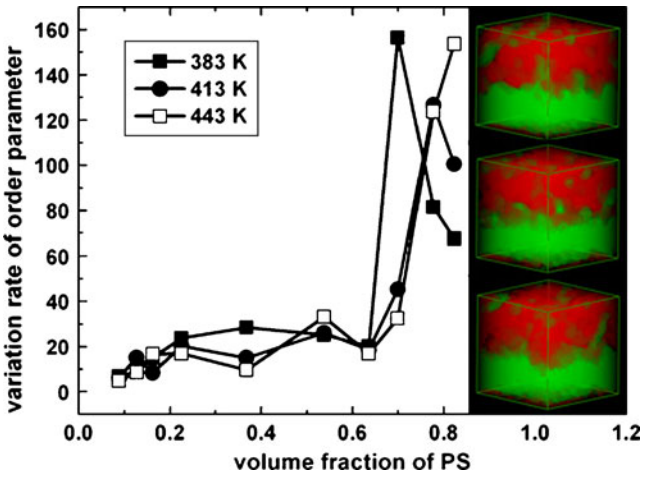

Fig. 9 *V ROP* data with the shear effect versus the volume fraction of PS. Isodensity surface pictures of an 8/1 (PS/PMMA) blend induced by a shear rate of 0.002 ns^{-1} are also shown, as are isodensity surface pictures of an 8/1 (PS/PMMA) blend at 443, 413 and 383 K (*top to bottom* in the chart, respectively). *Red*, PS; *green*, PMMA

Column-shaped nanoparticles were applied as an example. In order to determine the factor that exerts the most influence on phase separation, seven different kinds of nanoparticles were made for the doping study. In Table 2, the number of nanoparticles in each layer (N_p), the radius of each nanoparticle (r_p), the height of each nanoparticle (h_p), the number of layers (N_L) and the total number of nanoparticles doped (N_{tp}) are listed in detail. Among these cases, the 4-3-4-2 case (with four nanoparticles in each of two layers, a nanoparticle radius of 3 nm, and a nanoparticle height of 4 nm) was used as a reference, and all the other cases were derived from this. For example, adding only one more nanoparticle in the center resulted in the 4-3-4-3 case; increasing the number of layers to four but not changing any other settings yielded the 4-3-4-4 case; doubling the nanoparticle density of each layer produced the 8-3-4-2 case; doubling the nanoparticle height yielded the 4-3-8-2 case; adding one more nanoparticle to the middle of the simulation box and increasing the number of layers to three on the basis of the 4-3-8-2 case produced the 4-3-8-3 case; and doubling the nanoparticle radius on the basis of the 4-3-8-2 case gave the 4-6-8-2 case. The parameters chosen were the same as those used in the previous mesoscopic simulations; the χ value was that obtained at 400 K, and the total simulation time was 10 ms in each case. The simulation models were the plain PS/PMMA blends shown in Table 1.

Result and discussion

Figure 10 shows the *V ROP* values obtained for various kinds of nanoparticle doping situations. A few trends can be seen in these cases. First, the trends seen in these four pictures are almost the same. Second, since $V\,ROP_{1/3} > V\,ROP_{1/2} > V\,ROP_{2/1} > V\,ROP_{3/1}$, it can be deduced that the degree of phase separation intensifies with increasing PMMA content when the blend is rich in PMMA. Third, since $V\,ROP_{4\text{-}3\text{-}4\text{-}3} > V\,ROP_{4\text{-}3\text{-}4\text{-}2}$ and $V\,ROP_{4\text{-}3\text{-}8\text{-}3} > V\,ROP_{4\text{-}3\text{-}8\text{-}2}$, the order of the PS/PMMA blend increases when the number of nanoparticles of the same size is

Table 2 Mesoscopic simulations of PS/PMMA blends doped with nanoparticles

Simulation	Case	N_p	r_p (nm)	h_p (nm)	N_L	N_{tp}
1	4-3-4-2	4	3	4	2	8
2	4-3-4-3	4	3	4	3	9
3	4-3-4-4	4	3	4	4	16
4	4-3-8-2	4	3	8	2	8
5	4-3-8-3	4	3	8	3	9
6	4-6-8-2	4	6	8	2	8
7	8-3-4-2	8	3	4	2	16

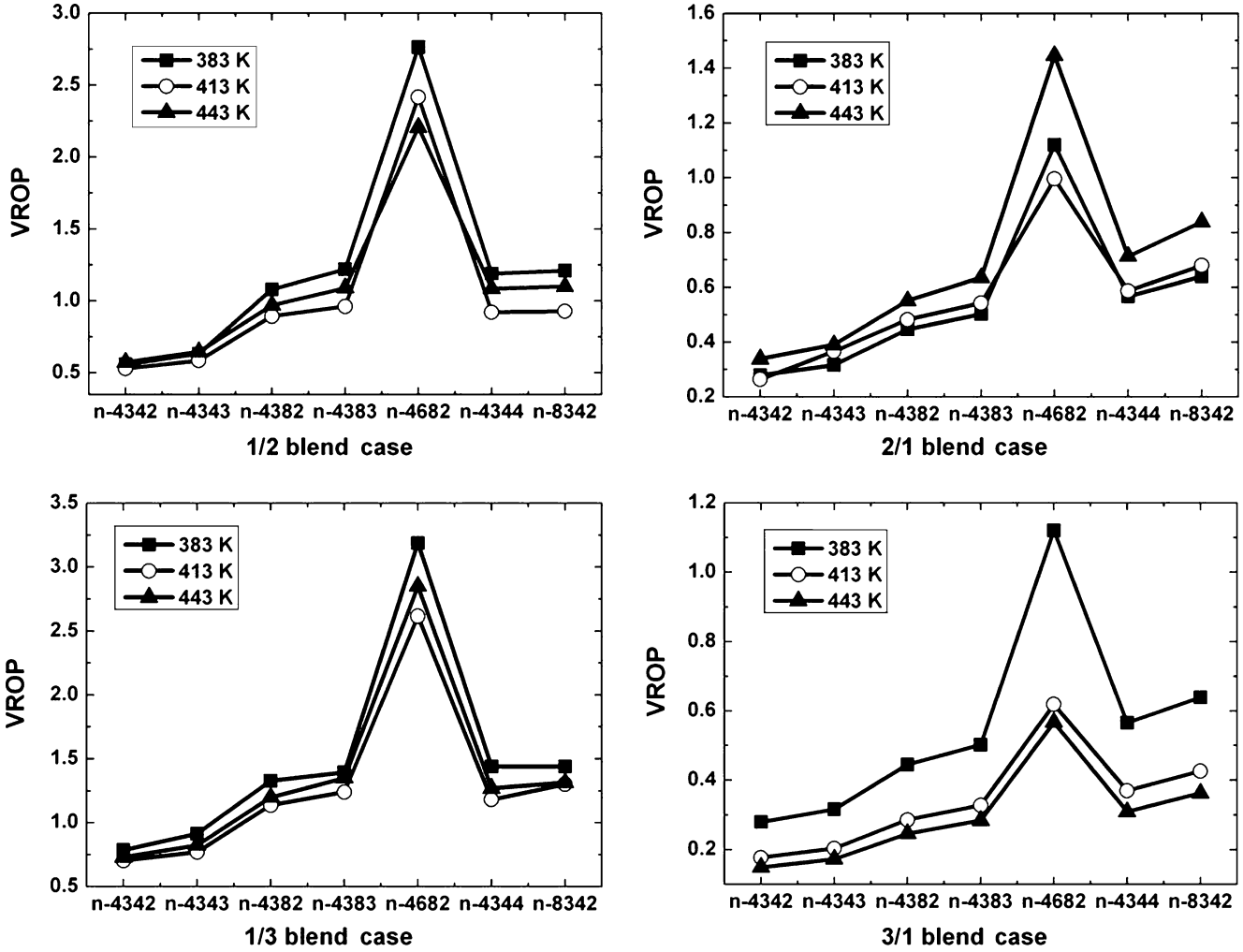

Fig. 10 *V ROP* data for the 1/2, 2/1 and the 1/3, 3/1 blend pairs doped with nanoparticles at 383, 413 and 443 K

increased. Fourth, since $V\ ROP_{8\text{-}3\text{-}4\text{-}2} > V\ ROP_{4\text{-}3\text{-}4\text{-}4}$, the order of the PS/PMMA blend can be increased by increasing the density of the nanoparticles of the same size. Fifth, it can be seen from the extremely high value of $V\ ROP_{4\text{-}6\text{-}8\text{-}2}$ that the nanoparticle size is the factor that exerts the most influence on the phase morphology.

From the third, fourth and fifth results discussed above ($V\ ROP_{4\text{-}6\text{-}8\text{-}2} \gg V\ ROP_{8\text{-}3\text{-}4\text{-}2} > V\ ROP_{4\text{-}3\text{-}4\text{-}4} > V\ ROP_{4\text{-}3\text{-}8\text{-}3} > V\ ROP_{4\text{-}3\text{-}8\text{-}2} > \mathrm{VROP}_{4\text{-}3\text{-}4\text{-}3} > V\ ROP_{4\text{-}3\text{-}4\text{-}2}$), we can see that the factors investigated had the following order of influence on the phase separation: nanoparticle size > nanoparticle density > number of doped nanoparticles.

Table 3 Mesoscopic simulations of PS/PMMA blends induced by "ci" and "co" planes

"ci" type	Row number (X-axis)	Row number (Y-axis)	Radius (nm)
ci-444	4	4	4
ci-882	8	8	2
"co" type	E/T^g (X-axis)	E/T^g (Y-axis)	Height (nm)
co-444	2/4	2/4	4
co-448	2/4	2/4	8
co-4412	2/4	2/4	12
co-4432	2/4	2/4	32
co-884	4/8	4/8	4
co-888	4/8	4/8	8
co-8812	4/8	4/8	12
co-8832	4/8	4/8	32

[g] This is the abbreviation for "effective/total row number."

Table 4 Mesoscopic simulations of PS/PMMA blends induced by "gra" and "rg" planes

"gra" type	Row number (X-axis)	Height (nm)	S^f in X-axis
gra-444	4	4,3,2,1	N
gra-888	8	8,7,6,5,4,3,2,1	N
gra-2(444)	8	4,3,2,1,1,2,3,4	Y
gra-2(448)	8	8,4,2,1,1,2,4,8	Y
gra-2(888)	16	8,7,6,5,4,3,2,1,1,2,3,4,5,6,7,8	Y
"rg" type	Layer number	Height (nm)	S^f in the X- and Y-axes
rg-442	2	2,4	Y
rg-884	4	8,4,2,1	Y
rg-16168	8	16,14,12,10,8,6,4,2	Y

[f] This is the abbreviation for "symmetry;" "N" means "no" and "Y" means "yes"

Furthermore, all of the PS/PMMA blend cases showed the same trends as those described above with nanoparticle doping.

PS/PMMA blends induced by various planes

To investigate which planes induce the most intense phase separation in PS/PMMA blends, four different types of inducing planes were designed as substrates using our own program. These four types were denoted "ci," "co," "gra," and "rg." The "ci" series of planes used half-spheres with different radii as a mask that simulated different degrees of surface roughness. The "co" series had equally spaced cubic columns as a mask. The columns had different sizes and heights to simulate different degrees of surface roughness. The "gra" series were planes with different widths to simulate different degrees of surface roughness. The mask was generated by gradually increasing the column height across the plane, so that it resembled stairs viewed side on. In addition, monodirectional asymmetric planes, such as gra-444 and gra-888, and monodirectional symmetric planes, such as gra-2(444), gra-2(448) and gra-2 (888), were considered. The "rg" series were bidirectional symmetric planes originating from monodirectional symmetric planes, as used in the "gra" series. Tables 3 and 4 describe these four types of planes used in the simulations, and Fig. 11 shows the eighteen planes pictorially.

Results and discussion

Figure 12 shows the *V ROP* values of PS/PMMA blends induced by the four types of planes mentioned above; eighteen isodensity surface pictures are shown for the 1/3 blend case at 413 K as examples at the top of each chart. The following trends can be discerned from these figures:

(1) For the "co" planes, $V\,ROP_{\text{co-8832}} > V\,ROP_{\text{co-8812}} > V\,ROP_{\text{co-888}} > V\,ROP_{\text{co-884}}$ and $V\,ROP_{\text{co-4432}} > V\,ROP_{\text{co-4412}} > V\,ROP_{\text{co-448}} > V\,ROP_{\text{co-444}}$, which shows that the PS/PMMA blends underwent more vigorous phase separation on rougher planes. The values of $V\,ROP_{\text{co-884}}$ and $V\,ROP_{\text{co-888}}$ were almost the same at 383, 413 and 443 K. The values of $V\,ROP_{\text{co-8812}}$ at 383 and 413 K were also the same, but the value of $V\,ROP_{\text{co-8812}}$ at 443 K jumped to 13.3, which was one order of magnitude higher than its values at 383 and 413 K. On a much rougher surface, such as a co-8832 type of plane, $V\,ROP_{\text{co-8832,443K}} > V\,ROP_{\text{co-8832,413K}} > V\,ROP_{\text{co-8832,383K}}$, which reveals that PS/PMMA blends undergo more intense phase separation at higher temperatures. The surfaces of the co-4xx series of planes were rougher than those of the co-8xx series of planes. The *V ROP* values of the co-4xx series were higher than those of the co-8xx series at 443 K, which is also consistent with the conclusion that more intense phase separation occurs on rougher planes.

(2) For the "ci" planes, $V\,ROP_{\text{ci-882}} > V\,ROP_{\text{ci-444}}$ at the same temperature. There was no obvious difference between the $V\,ROP_{\text{ci-882}}$ values at 383 and 443 K, and there was no obvious difference between the $V\,ROP_{\text{ci-444}}$ values at 383 and 443 K either. Furthermore, the $V\,ROP_{\text{ci-882}}$ and $V\,ROP_{\text{ci-444}}$ values at 413 K were both higher than their corresponding values at lower (383 K) or higher (443 K) temperatures. This shows that temperature is the most influential factor on the phase separation of PS/PMMA blends induced by "ci" planes, but also that the *V ROP* values vary irregularly with temperature. Both the temperature and the degree of surface roughness contribute to the results.

(3) For the "rg" planes, the same order of $V\,ROP_{\text{rg-16168}} > V\,ROP_{\text{rg-884}} > V\,ROP_{\text{rg-442}}$ was seen at three temperatures, which shows that the degree of surface roughness is an important factor for inducing phase separation, especially for rougher planes with high step gradients, such as rg-16168. Nearly the same value of $V\,ROP_{\text{rg-442}}$ was observed at 383 and 443 K—the same situation as seen for $V\,ROP_{\text{rg-884}}$—so it can be presumed that for the smoother planes, such as rg-884 and rg-442, temperature is more important than the degree of surface roughness in inducing phase separation.

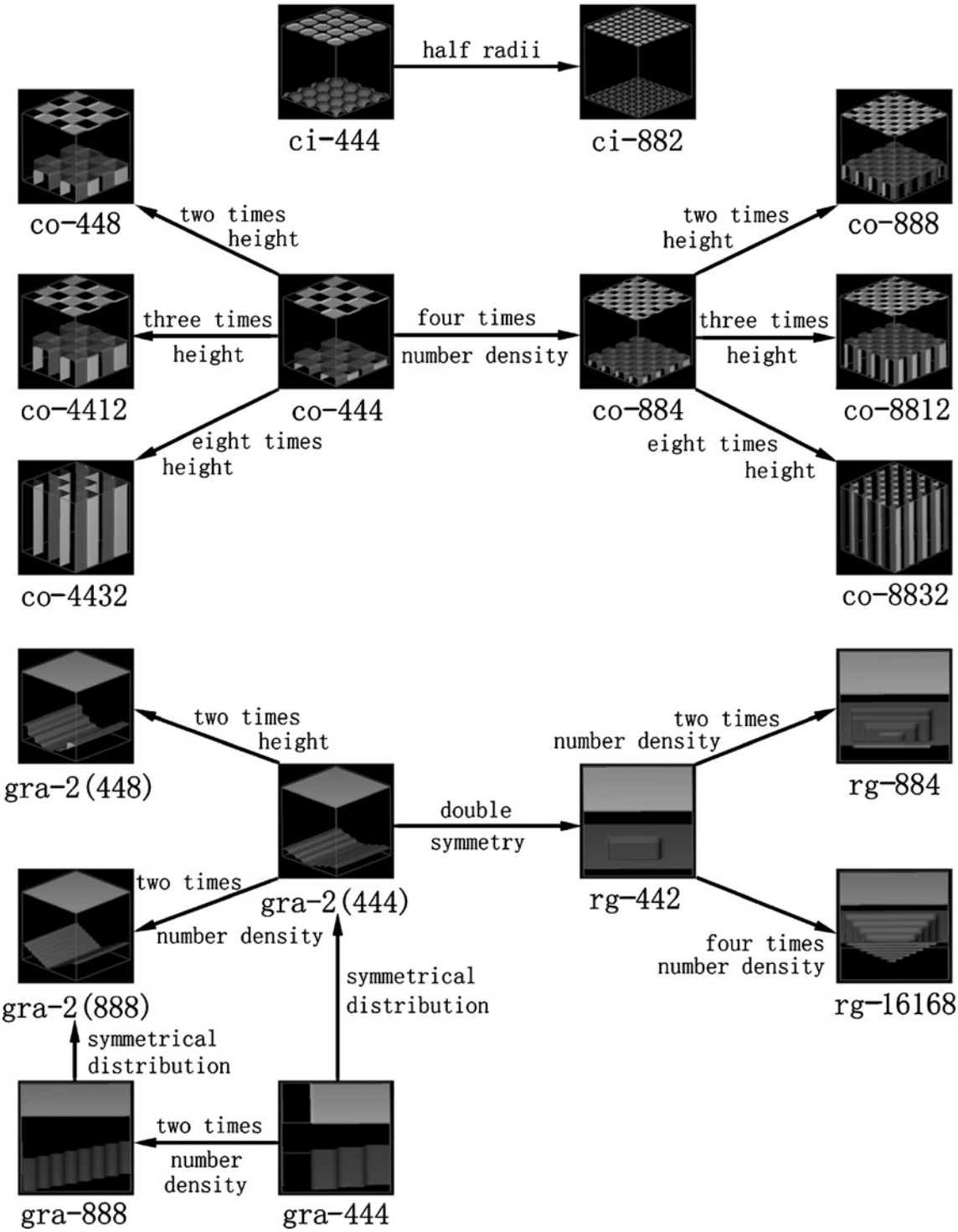

Fig. 11 The four types of plane used in the simulations: "ci," "rg," "gra," and "co"

(4) For the "gr" planes, the *V ROP* values for gr-444 were lower than those for other "gr" planes at 383, 413 and 443 K, and all of these planes presented similar values at 383 and 443 K; in addition, the other "gr" planes except for gr-444 presented nearly the same *V ROP* values at 383, 413 and 443 K. This shows that the degree of surface roughness plays a small role in inducing phase separation for "gr" planes. In contrast, it can be deduced from the extremely high value of *V ROP* at 413 K that temperature is the main inducing factor for these planes.

(5) For all of the "ci," "rg," and "gr" planes, the *V ROP* values at 413 K were much higher than those at 383

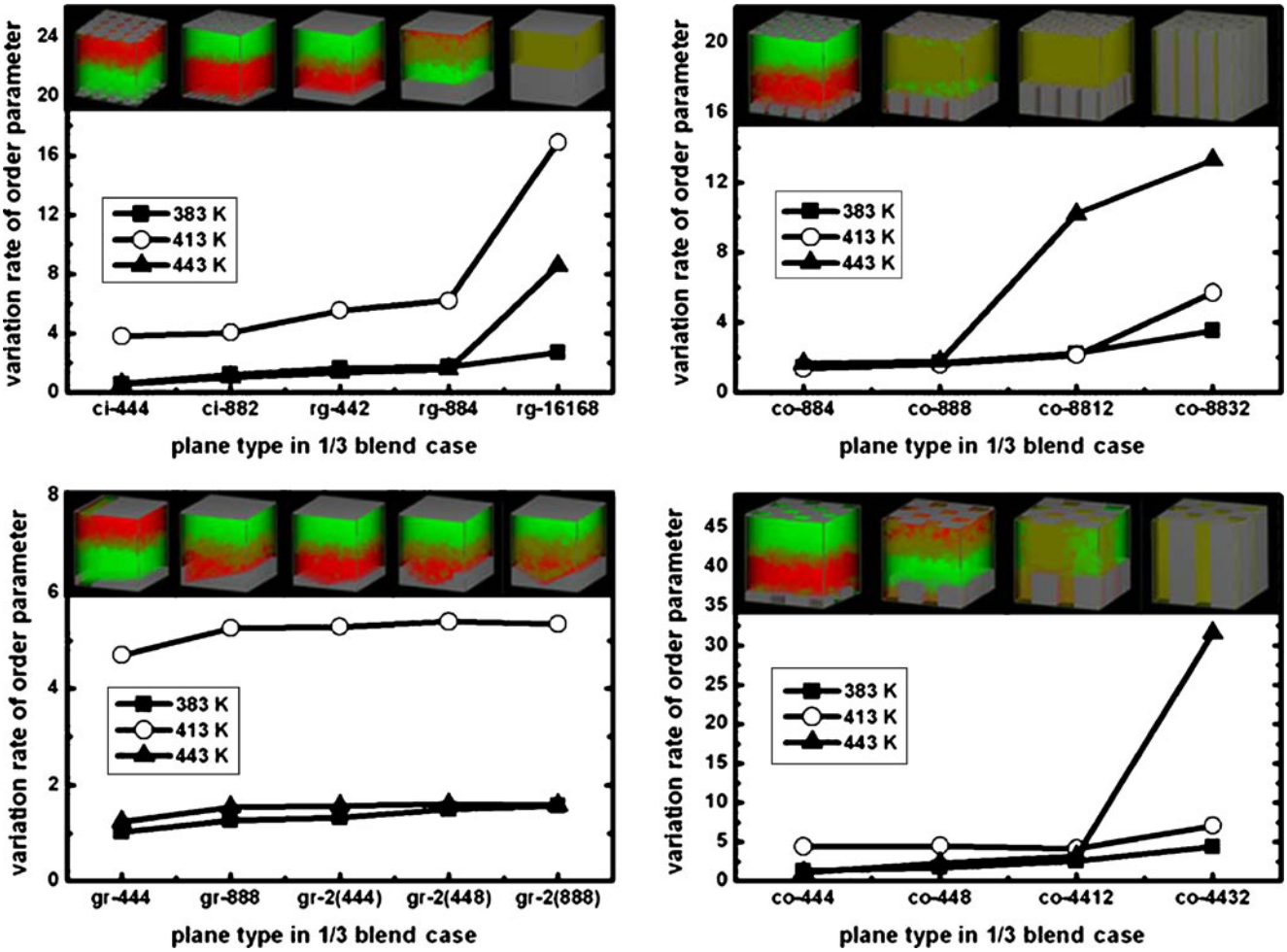

Fig. 12 *V ROP* data for the 1/3 blend case at 383, 413 and 443 K, respectively. Isodensity surface pictures are shown for PS/PMMA blends induced by different types of planes at 413 K. *Red*, PS; *green*, PMMA

and 443 K; furthermore, the *V ROP* values at 383 and 443 K were nearly the same for each plane, which reveals that using a higher (443 K) or lower (383 K) temperature had nearly the same effect on phase separation, and that there was a "critical" temperature between 443 and 383 K (such as 413 K) that could induce the most vigorous phase separation. The influence of each "ci," "rg," or "gr" plane on phase separation mainly depended on this critical temperature, not on the degree of surface roughness, in contrast to what was seen for the "co" planes.

The "ci," "rg," and "gr" planes were different from the "co" planes in that the first three types of plane had continuous mask distributions on their surfaces, which allowed the PS/PMMA blends to move and spread more freely until they could adjust themselves to reach stable phase separation. In contrast, the "co" planes did not have continuous mask distributions on their surfaces, which meant that the polymer did not have enough room to move and spread; they could only adjust themselves in the "small cubic spaces" formed by neighboring column masks. Furthermore, the big difference between the diffusion abilities of PS and PMMA was also a barrier to movement and adjustment. Because of the two reasons mentioned above, the degrees of phase separation differed widely between the first three types of plane and the "co" planes.

Conclusion

The two most important processes during the MD simulation are the annealing process after minimization and the MD simulations with three NVT and NPT ensemble cycles. The strong polymer end–end interactions, which evidently influence the simulation results, can only be reduced by performing the above two processes. Based on the calculated δ values for different numbers of repeating units of PS and PMMA, their representative chain lengths were found to be 30 and 60, respectively. By comparing the

calculated χ with $\chi_{critical}$, it was found that the PS/PMMA blends were immiscible in our simulations. Furthermore, the χ data did not depend greatly on the simulation temperatures.

The input parameters used in MesoDyn were derived from the MD simulations, and mesoscopic simulations were carried out at 383, 413 and 443 K. After calculating the *V ROP* values of ten different representative composition cases with block copolymer added, two outstanding features were found. First, the PS-rich blend cases at higher simulation temperatures, such as 413 and 443 K, underwent a more obvious phase separation in microscopic phase morphology. Second, when the 1/1 blend case was used as the reference, the symmetric blend pairs, such as 1/2, 2/1 and 1/3, 3/1, etc., gradually showed miscibility as the temperature was increased.

Mesoscopic simulations were then carried out on PS/PMMA blends with shear stress factored in. The results of those simulations showed that this shearing was a good way of inducing phase separation, especially in PS-rich blends. Here, the temperature was not found to be an important factor in phase separation, especially for the PMMA-rich blends.

Next, mesoscopic simulations were carried out on plain PS/PMMA blends doped with various numbers and densities of nanoparticles of various sizes. The simulation results showed that nanoparticle doping was an effective way of improving the degree of order in the microscopic phases, especially in the PMMA-rich blends. No matter which PS/PMMA blend composition was considered, the nanoparticle size had a stronger influence on the phase morphology than the density of nanoparticles, and the density of nanoparticles had a stronger influence than the number of nanoparticles.

Finally, in order to research the effects of various planes on the phase separation of PS/PMMA blends, four types ("ci," "rg," "gr" and "co") of planes were constructed. For the first three types of planes, the degree of surface roughness played only a small role in inducing phase separation: the temperature was the most important factor in this respect. Furthermore, there was a "critical" temperature between 443 and 383 K (such as 413 K) at which the phase separation occurred most intensely. However, rougher planes and higher temperatures both helped to induce phase separation on "co" planes.

References

1. Paul DR, Newman S (1978) Polymer blends. Academic, New York
2. Abd-El-Messieh SL (2003) Polym Plast Technol Eng 42(1):153–169
3. Schneider IA, Calugaru EM (1976) Eur Polym J 12(12):879–881
4. Bada R, Perez Jubindo MA, De LA, Fuente MR (1987) Mater Chem Phys 18(4):359–373
5. Zhu PP (1997) Eur Polym J 33(3):411–413
6. Lee JK, Han CD (1999) Polymer 40:6277–6296
7. Lee CF (2000) Polymer 41(4):1337–1344
8. Li X, Han YC, An LJ (2003) Polymer 44(26):8155–8165
9. Walheim S, Boltau M, Mlynek J, Krausch G, Steiner U (1997) Macromolecules 30:4995–5003
10. Schmidt JJ, Gardella JA Jr, Salvati L Jr (1989) Macromolecules 22:4489–4495
11. Chiou JS, Barlow JW, Paul DR (1987) J Polym Sci Part B Polym Phys 25:1459–1471
12. Lhoest JB, Bertrand P, Weng LT, Dewez JL (1995) Macromolecules 28:4631–4637
13. Davies MC, Shakesheff KM, Shard A, Domb A, Roberts CJ, Tendler SJB, Williams PM (2000) Macromolecules 29:2205–2212
14. Schreiber HP (1993) Aspects of component interactions in polymer systems: the interfacial interactions in polymeric composites. Kluwer, Boston
15. Buki L, Gonczy E, Fekete E, Hellmann GP, Pukanszky B (2001) Macromol Symp 170:9–20
16. Lodge TP, Wood ER, Haley JC (2006) J Polym Sci Part B Polym Phys 44:756–763
17. Valls OT, Farrell JE (1993) Phys Rev E 47:R36–R39
18. Ramirez-Piscina L, Hernandéz-Machado A, Sancho JM (1993) Phys Rev B 48:125–131
19. Kawakatsu T, Kawasaki K, Furusaka M, Okabayashi H, Kanaya T (1993) J Chem Phys 99(10):8200–8217
20. Shinozaki A, Oono Y (1993) Phys Rev E 48:2622–2654
21. Fraaije JEM (1993) J Chem Phys 99:9202–9212
22. Fraaije JGEM, van Vlimmeren BAC, Maurits NM, Postma M, Evers OA, Hoff-man C, Altevogt P, Goldbeck-Wood G (1997) J Chem Phys 106:4260–4269
23. Jawalkar SS, Adoor SG, Sairam M, Nadagouda MN, Aminabhavi TM (2005) J Phys Chem B 109(32):15611–15620
24. Groot RD, Warren PB (1997) J Chem Phys 107:4423–4435
25. Groot RD, Madden TJ (1998) J Chem Phys 108:8713–8724
26. Mu D, Huang XR, Lu ZY, Sun CC (2008) Chem Phys 348:122–129
27. Flory PJ (1989) Statistical mechanics of chain molecules. Munich, Germany
28. Mark JE (1999) Polymer data handbook. Oxford University Press, New York
29. Brandrup J, Immergut EH, Grulke EA (1999) Polymer handbook, 4th edn. Wiley, New York
30. Hoover WG (1985) Phys Rev A 31:1695–1697
31. Rigby D, Sun H, Eichinger BE (1997) Polym Int 44:311–330
32. Sun H (1998) J Phys Chem B 102:7338–7364
33. Sun H, Ren P, Fried JR (1998) Comput Theor Polym Sci 8:229–246
34. Ewald PP (1921) Ann Phys 64:253–287
35. Grulke EA (1999) Solubility parameter values. In: Polymer handbook, 4th edn. Wiley, New York
36. Calahorra E, Cortazar M, Guzman GM (1985) J Polym Sci Polym Lett Ed 23:257–260
37. Krause S, Paul DR, Newman S (1978) Polymer–polymer compatibility in polymer blends, vol 1. Academic, New York
38. Fan CF, Cagin T, Chen ZM, Smith KA (1994) Macromolecules 27:2383–2391